

Dephasing of Majorana qubits due to quasistatic disorder

Péter Boross^{1,2} and András Pályi²

¹*Institute for Solid State Physics and Optics, Wigner Research Centre for Physics, H-1525 Budapest P.O. Box 49, Hungary*

²*Department of Theoretical Physics and MTA-BME Exotic Quantum Phases Research Group,
Budapest University of Technology and Economics, H-1111 Budapest, Hungary*

(Dated: March 10, 2022)

Quantum bits based on Majorana zero modes are expected to be robust against certain noise types, and hence provide a quantum computing platform that is superior to conventional qubits. This robustness is not complete though: imperfections can still lead to qubit decoherence and hence to information loss. In this work, we theoretically study Majorana-qubit dephasing in a minimal model: in a Kitaev chain with quasistatic disorder. Our approach, based on numerics as well as first-order non-degenerate perturbation theory, provides a conceptually simple physical picture and predicts Gaussian dephasing. We show that, as system parameters are varied, the dephasing rate due to disorder oscillates out-of-phase with respect to the oscillating minigap of the clean system. In our model, first-order dephasing sweet spots are absent, a feature that can be used to characterize the spatial structure of noise in a dephasing experiment. We expect that our results will be utilized for the design and interpretation of future Majorana-qubit experiments.

I. INTRODUCTION

Theoretical proposals^{1–3} suggest that Majorana zero modes (MZMs) can be engineered in quasi-one-dimensional semiconducting-superconducting hybrid systems^{4,5}. The past decade has witnessed intense experimental activities to establish MZMs^{4,6–20}. It is expected that MZMs could serve as building blocks in experiments demonstrating topologically protected quantum memories, quantum dynamics, or even quantum computing^{21–28}. In that context, understanding the decoherence of Majorana qubits^{26,29–40} is an important task.

The minimal model hosting MZMs is the Kitaev chain⁴¹. It can be used to describe the dephasing process of a Majorana qubit. The ground state of a finite-length topological Kitaev chain hosts two MZMs at the two ends of the chain, implying that the ground state is approximately twofold degenerate, with one ground state being of even fermion parity and the other being of odd fermion parity. In a chain with a finite length, a small energy minigap separates the two ground states. If random components, such as disorder^{29,42}, are incorporated in the model, then the minigap becomes a random variable. To encode a single qubit with MZMs, two wires and hence four MZMs are needed⁴³. In such a two-wire Majorana qubit, the random minigaps in the two wires add up to a random Larmor frequency of the qubit, leading to qubit dephasing.

In this work, we theoretically study dephasing of Majorana qubits in the presence of slow charge noise. A key target in topological quantum computing is the experimental demonstration of a topologically protected quantum memory based on MZMs, hence it is imperative to understand the potential sources of qubit decoherence, to assess future device functionality and provide optimization guidelines. Furthermore, qubit dephasing measurement is an established tool to reveal the noise structure of the qubit’s environment^{44–47}; understanding de-

phasing is important for that application, too. In our work, we focus on the model of quasistatic disorder^{48–53}, a minimal model of slow (low-frequency) charge noise or $1/f$ noise^{40,44,46,47,54–57}, which has been a very important source of qubit dephasing both in semi- and superconductor environments.

Naturally, Majorana qubit dephasing due to weak and slow (quasistatic) charge noise is determined by the probability distribution of the minigap, see, e.g., our section V. We will study that minigap distribution by both numerical and analytical methods, and show that it is Gaussian for weak disorder. We argue that this result is consistent with the log-normal minigap-envelope distribution found by Ref. 29 in our Appendix B.

Having the minigap distribution at hand, we use it to characterize the dephasing of a Majorana qubit subject to weak quasistatic disorder. In simple models, the time dependence of qubit dephasing often follows a Gaussian function^{26,58}. Here we show that this is also the case for the qubit studied here. Key results are that (i) we provide an analytical formula for the dephasing susceptibility [see Eq. (29)] and the dephasing time [see Eq. (38)], (ii) we reveal an out-of-phase oscillation between the minigap of the clean system and the dephasing susceptibility to disorder [see Fig. 2b and Fig. 4a-b], (iii) and we highlight the absence of dephasing sweet spots in our model (see Sec. V).

The rest of the paper is organized as follows. In section II, we show numerical results for the minigap distribution of the disordered chain, highlighting the Gaussian distribution of the minigap, and the out-of-phase oscillation between the clean minigap and the minigap susceptibility to disorder. In section III, we use the continuum version of the Kitaev chain, together with mode matching and first-order perturbation theory, to establish the semi-analytical description of the minigap distribution, and to derive approximate analytical results for that. In section IV, we relate the Kitaev chain to its continuum version and compare the corresponding results. In section V,

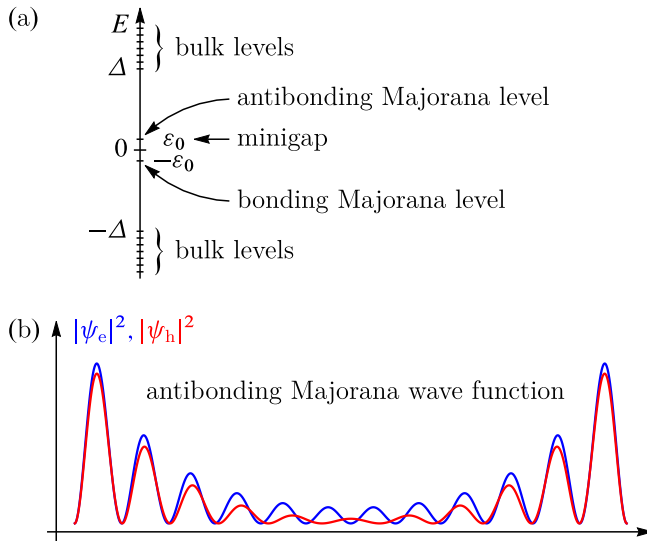


FIG. 1. Spectrum and Majorana wave functions in a topological superconductor wire. (a) Schematic spectrum of the Bogoliubov-de Gennes matrix. (b) Electron and hole components of the antibonding Majorana wave function

we relate the minigap distribution and the dephasing dynamics of a Majorana qubit based on two Kitaev chains. We discuss implications and follow-up ideas in section VI, and conclude in section VII.

II. DISORDER-INDUCED MINIGAP DISTRIBUTION IN THE KITAEV CHAIN

We use the Kitaev-chain tight-binding model⁴¹ to numerically investigate Majorana qubit dephasing. In this section, we numerically determine the disorder-induced distribution of the signful minigap (see definition below), using the Kitaev chain. We anticipate that this distribution is Gaussian for weak quasistatic disorder (see below within this section for details), and that the Majorana qubit dephasing time T_2^* in a two-chain setup is determined by the standard deviation σ_{ε_0} of the signful minigap ε_0 [see Eq. (38) in section V].

The Hamiltonian of a finite-length Kitaev chain in real space reads⁴¹

$$H_K = - \sum_{n=1}^N \left(\mu_K + \delta\mu_n^{(K)} \right) c_n^\dagger c_n - t \sum_{n=1}^{N-1} \left(c_n^\dagger c_{n+1} + \text{h.c.} \right) - \Delta_K \sum_{n=1}^{N-1} \left(c_n c_{n+1} + \text{h.c.} \right), \quad (1)$$

Parameter/scale	Notation	Value
Continuum model		
Effective mass (of InAs)	m	$0.023m_e$
Chemical potential	μ_C	1 meV
Superconducting gap	Δ_C	$200 \mu\text{eV}$
Kitaev chain		
Normal hopping amplitude	t	6.62 eV
Lattice constant	a	0.5 nm
Chemical potential	μ_K	-13.3 eV
Superconducting pairing potential	Δ_K	8.14 meV
Length scales		
Fermi-wavelength	λ_F	$511a$
Fermi-wavenumber	k_F	$0.0123/a$
Superconductor coherence length	ξ	$814a$
Inverse coherence length	κ	$0.00123/a$

TABLE I. Parameter values used in the numerical and analytical calculations.

where c_n^\dagger and c_n are the electron creation and annihilation operator on site n , respectively, t is the hopping amplitude, μ_K is the chemical potential, Δ_K is the superconducting pair potential, and N is the number of sites. We model disorder as a random on-site potential, independent on each site, drawn from Gaussian distribution with zero mean and standard deviation σ_μ , that is, $\delta\mu_n^{(K)} \sim \mathcal{N}(0, \sigma_\mu)$. For a discussion of the relation between this model and disorder in real samples, see section VI.

We obtain the minigap ε_0 using the Bogoliubov-de Gennes (BdG) transformation⁵⁹, i.e., by numerically finding the smallest positive eigenvalue of the corresponding real-space $2N \times 2N$ BdG Hamiltonian⁶⁰. We will calculate the minigap ε_0 for a clean system, i.e., in the absence of any disorder, as well as for random on-site disorder realizations. In the latter case, ε_0 becomes a random variable – with Gaussian distribution for weak disorder, as shown in Fig. 2a and discussed below.

A clean Kitaev chain has a minigap that decreases in an oscillatory fashion as the chain length is increased^{61–64}. This is shown in Fig. 2b, where we plot the numerically calculated length dependence of ε_0 (red solid line) for a parameter set shown in the ‘Kitaev chain’ section of Table I.

Now we introduce disorder and study the minigap distribution. Figure 2a shows three examples of that distribution, for a fixed disorder strength $\sigma_\mu = 100 \mu\text{eV}$, for three different chain lengths $N = 2000, 3000, 4000$. The figure clearly shows a Gaussian character for all three distributions. Furthermore, the figure also shows the trend that both the mean and the standard deviation of these distributions decrease as the chain length increases.

Figure 2c shows a more systematic analysis of the length- and disorder-strength dependence of the standard deviation σ_{ε_0} of the signful minigap ε_0 . Note the difference between the *signful minigap* ε_0 and the *minigap* ε_0 . The signful minigap is defined by $\varepsilon_0 \equiv \varepsilon_0 - \varepsilon_e$, where ε_0 (ε_e) is the energy of the odd (even) ground state. We have

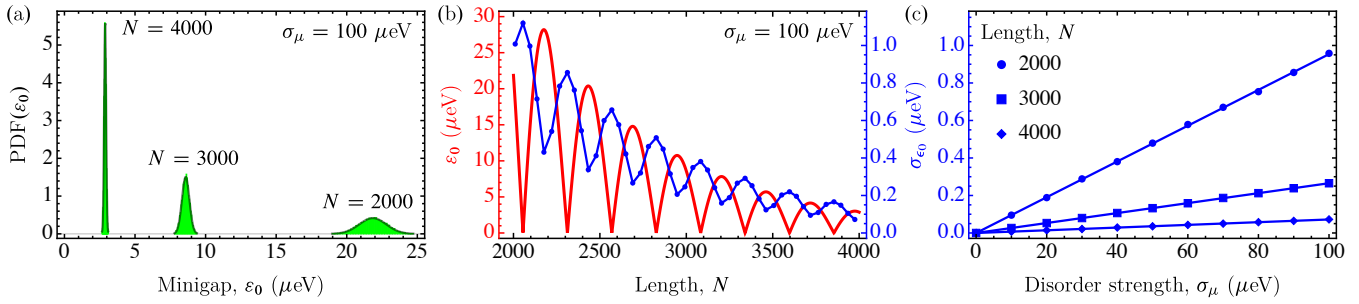


FIG. 2. Minigap, its probability distribution and its standard deviation from the Kitaev chain model. (a) Numerically obtained probability density functions (pdfs) of the minigap for three different lengths in disordered system. Gray lines are fitted Gaussian pdfs. (b) Minigap of the clean system (red line) and standard deviation of the signful minigap (blue points) are shown as a function of chain length, for the disorder strength $\sigma_\mu = 100 \mu\text{eV}$. Out-of-phase oscillation can be observed between the minigap and its standard deviation. (c) Standard deviation of the signful minigap is shown as a function of the strength of the on-site disorder for three different lengths. The dependence on the disorder strength is linear for the shown range. Results for disordered systems are calculated using 10000 realizations.

defined the minigap (see Fig. 1a) as the absolute value of the signful minigap, i.e. $\varepsilon_0 \equiv |\epsilon_0|$. The distinction between ε_0 and ϵ_0 is motivated by the observation that the dephasing dynamics is related to the signful minigap ε_0 , see Eq. (38).

For all lengths displayed in Fig. 2c, the standard deviation σ_{ε_0} of the signful minigap shows a clear linear dependence on the disorder strength σ_μ . This linear dependence motivates the definition of the dimensionless *dephasing susceptibility to disorder*, $\chi = \sigma_{\varepsilon_0}/\sigma_\mu$. In Eq. (28), we will provide an approximate analytical formula for this susceptibility.

The Gaussian character of the minigap distribution, and the linear dependence of the minigap standard deviation on the disorder strength can be qualitatively understood in three steps. We briefly summarize these here, and will use these considerations in the next section in our quantitative derivations.

(1) The bonding and antibonding Majorana levels, see Fig. 1a, are particle-hole symmetric partners of each other. This implies that disorder (or any other perturbation) can not couple them directly.

(2) Therefore, there is no need to use degenerate or quasi-degenerate perturbation theory to describe the leading-order effect of disorder on the energy levels. It is sufficient to do first-order non-degenerate perturbation theory for, say, the antibonding level. This explains the linear dependence of the minigap standard deviation on the disorder strength.

(3) The first-order perturbative description implies that the first-order energy correction $\delta\varepsilon_0^{(1)}$ due to disorder in our model (independent random on-site energies) is a sum of many independent random variables for long chains, $N \gg 1$, and hence the central limit theorem ensures the Gaussian character of that energy correction.

Finally, we point out an out-of-phase oscillation effect between the standard deviation σ_{ε_0} of the signful minigap and the clean minigap ε_0 . In Fig. 2b, the blue points show the length dependence of the standard deviation

σ_{ε_0} of the signful minigap, for the disorder strength $\sigma_\mu = 100 \mu\text{eV}$. Note that the y axis for these blue points is the right y axis which is also colored blue. Fig. 2b shows that the minigap standard deviation σ_{ε_0} oscillates and decays as the length increases, similarly to the minigap of the clean system. However, there is an out-of-phase oscillation between the minigap and its disorder-induced standard deviation: e.g., the standard deviation has a maximum wherever the minigap reaches zero.

Note that with our numerical approach, it is straightforward to estimate the standard deviation σ_{ε_0} of the minigap; however, Majorana-qubit dephasing is determined by the standard deviation σ_{ε_0} of the signful minigap [Eq. (38)]. To estimate the latter, we do the following. If the expectation value of the minigap ε_0 is much larger than its standard deviation, then $\sigma_{\varepsilon_0} \approx \sigma_{\varepsilon_0}$, hence we use the minigap statistics to estimate σ_{ε_0} . If the above condition does not hold, then we convert the statistics of the minigap to the statistics of the signful minigap, and from the latter we estimate σ_{ε_0} , as described in Appendix A.

III. MINIGAP IN THE CONTINUUM VERSION OF THE KITAEV CHAIN

Numerical computation of the minigap from the Kitaev chain model or other tight-binding models can be computationally expensive for larger system size. To establish a more efficient calculational tool, and to enable analytical results for the minigap absolute value and its standard deviation, here we study the continuum version of the Kitaev chain. These analytical results serve also as a benchmark against which the numerical results can be checked.

First, we use mode matching to obtain the BdG wave function of the quasi-zero-energy mode in a clean (disorder-free) wire.⁶³ Second, we use this wave function and first-order non-degenerate perturbation theory to de-

termine the standard deviation σ_{ϵ_0} of the minigap.

A. Minigap and antibonding Majorana wave function in a clean wire

The continuum model has the following momentum-space Hamiltonian²⁹:

$$\mathcal{H}_C(k) = \left(\frac{\hbar^2 k^2}{2m} - \mu_C \right) \sigma_z - \Delta'_C \hbar k \sigma_x, \quad (2)$$

where m is the effective mass, μ_C is the chemical potential, and σ_x and σ_z are Pauli matrices acting in Nambu space. The index C stands for ‘continuum’. For future use, we define

$$k_F = \sqrt{2m\mu_C}/\hbar, \quad (3a)$$

$$v_F = \hbar k_F/m, \quad (3b)$$

$$\Delta_C = \Delta'_C \hbar k_F, \quad (3c)$$

$$\xi = \hbar v_F/\Delta_C, \quad (3d)$$

where k_F is the Fermi wave number, v_F is the Fermi-velocity, Δ_C is the superconducting gap and ξ is the superconductor coherence length. We will describe a finite-length wire with length L and hard-wall boundary conditions. The relation of this Hamiltonian and the Kitaev-chain Hamiltonian is detailed in Sec. IV.

We use mode-matching to determine the Majorana antibonding state and its energy (the minigap). The first step is to establish the evanescent modes close to zero energy in a homogeneous system. With that aim, we insert the standard plane-wave ansatz to the BdG equation $\mathcal{H}_C(-i\partial_x)\psi(x) = \varepsilon\psi(x)$ defined by Eq. (2).

It is straightforward to show that this approach yields four evanescent solutions for energies $0 \leq \varepsilon < \sqrt{\Delta_C^2 - (\Delta_C^2/2\mu_C)^2}$, with complex wave numbers $k_1 = K + i\kappa$, $k_2 = -K + i\kappa$, $k_3 = K - i\kappa$ and $k_4 = -K - i\kappa$. Here

$$K = \frac{1}{\hbar} \sqrt{m \left(\sqrt{\mu_C^2 - \varepsilon^2} + \mu_C - \frac{\Delta_C^2}{2\mu_C} \right)}, \quad (4a)$$

$$\kappa = \frac{1}{\hbar} \sqrt{m \left(\sqrt{\mu_C^2 - \varepsilon^2} - \mu_C + \frac{\Delta_C^2}{2\mu_C} \right)}. \quad (4b)$$

Furthermore, K and κ are positive numbers for $0 \leq \varepsilon < \sqrt{\Delta_C^2 - (\Delta_C^2/2\mu_C)^2}$. The corresponding non-normalized

wave functions have the form

$$\psi_{k_i}(x) = \begin{pmatrix} u_{k_i} \\ v_{k_i} \end{pmatrix} e^{ik_i x} = \begin{pmatrix} \Delta'_C \hbar k_i \\ \frac{\hbar^2 k_i^2}{2m} - \mu_C - \varepsilon \end{pmatrix} e^{ik_i x}, \quad (5)$$

where u_{k_i} and v_{k_i} represent the electron and hole components of the wave function in the momentum space.

The antibonding Majorana wave function must be a linear superposition of the four evanescent modes at a given energy:

$$\psi(x) = \begin{pmatrix} \psi_e(x) \\ \psi_h(x) \end{pmatrix} = \sum_{i=1}^4 \alpha_i \begin{pmatrix} u_{k_i} \\ v_{k_i} \end{pmatrix} e^{ik_i x}, \quad (6)$$

where $\psi_e(x)$ and $\psi_h(x)$ are the electron and hole components of the Majorana bound state, furthermore α_i -s are complex coefficients. This wave function $\psi(x)$ must satify the hard-wall boundary conditions:

$$\psi(0) = \psi(L) = \begin{pmatrix} 0 \\ 0 \end{pmatrix}. \quad (7)$$

This condition is fulfilled by coefficient vectors satisfying the following homogeneous linear set of equations:

$$\mathcal{M} \begin{pmatrix} \alpha_1 \\ \alpha_2 \\ \alpha_3 \\ \alpha_4 \end{pmatrix} = \begin{pmatrix} 0 \\ 0 \\ 0 \\ 0 \end{pmatrix}, \quad (8)$$

where the ε -dependent matrix \mathcal{M} is defined as

$$\mathcal{M} = \begin{pmatrix} u_{k_1} & u_{k_2} & u_{k_3} & u_{k_4} \\ v_{k_1} & v_{k_2} & v_{k_3} & v_{k_4} \\ u_{k_1} e^{ik_1 L} & u_{k_2} e^{ik_2 L} & u_{k_3} e^{ik_3 L} & u_{k_4} e^{ik_4 L} \\ v_{k_1} e^{ik_1 L} & v_{k_2} e^{ik_2 L} & v_{k_3} e^{ik_3 L} & v_{k_4} e^{ik_4 L} \end{pmatrix}. \quad (9)$$

As follows from Eq. (8), for a given length L , the condition

$$\det(\mathcal{M}(\varepsilon)) = 0 \quad (10)$$

gives the energy ε_0 of the antibonding Majorana state. In general, Eq. (10) leads a transcendental equation, which can be solved numerically: $\varepsilon_{0,\text{num}}$. Power-series expansion of $\det(\mathcal{M})$ in ε up to second order provides an analytical solution that in the limit of $L \gg 1/k_F, \xi$ reads

$$\varepsilon_0(L) \approx 2\Delta_C k_F e^{-L/\xi} \left| \frac{\sin \left(\sqrt{k_F^2 - 1/\xi^2} L \right)}{\sqrt{k_F^2 - 1/\xi^2}} \right|, \quad (11)$$

where we use $K|_{\varepsilon=0} = \sqrt{k_F^2 - 1/\xi^2}$ and $\kappa|_{\varepsilon=0} = 1/\xi$.

Depending on the relative magnitude of k_F and $1/\xi$, from Eq. (11) we obtain

$$\varepsilon_0(L) \approx \begin{cases} \Delta_C \frac{2k_F}{\sqrt{k_F^2 - 1/\xi^2}} e^{-L/\xi} \left| \sin \left(\sqrt{k_F^2 - 1/\xi^2} L \right) \right|, & \text{if } k_F > 1/\xi, \\ \Delta_C \frac{k_F}{\sqrt{1/\xi^2 - k_F^2}} e^{-\left(1/\xi - \sqrt{1/\xi^2 - k_F^2}\right)L}, & \text{if } k_F < 1/\xi. \end{cases} \quad (12a)$$

$$(12b)$$

If $k_F > 1/\xi$ (i.e. when $\mu_C > \Delta_C/2$), the minigap has an oscillatory part, but if $k_F < 1/\xi$, the minigap decreases purely exponentially as the length increases. For a physically feasible parameter set shown in Table I, including a chemical potential (e.g., set by a gate voltage) $\mu_C = 1$ meV, we obtain $k_F > 1/\xi$. This is the case we focus on from now on. To reach $k_F < 1/\xi$, the chemical potential needs to be suppressed as $0 < \mu_C < 0.1$ meV; we do not treat this case here.

Our result (12a) is in fact a generalization of an earlier result, see below Eq. (5) in Ref. 62. The only difference is the appearance of $\sqrt{k_F^2 - 1/\xi^2}$ in our result. The earlier result can be obtained by taking the limit $k_F \gg 1/\xi$ of our formula (12a), i.e., by applying the approximation $\sqrt{k_F^2 - 1/\xi^2} \approx k_F$.

Next, we describe the antibonding Majorana wave function. To simplify the description, we utilize the symmetries of the setup. The clean system has inversion symmetry. The corresponding operator has the form $\Pi = \pi \otimes \sigma_z$, where π is the inversion with respect to the point $x = L/2$, acting in real space, and σ_z acts in Nambu space. Inversion symmetry, together with the assumption that the antibonding Majorana energy level is

non-degenerate, implies that

$$\begin{pmatrix} \psi_e(x) \\ \psi_h(x) \end{pmatrix} = \begin{pmatrix} \pm \psi_e(L-x) \\ \mp \psi_h(L-x) \end{pmatrix}. \quad (13)$$

The Hamiltonian Eq. (2) also has bosonic time-reversal symmetry with the operator $T = (\mathbb{1} \otimes \sigma_z)\mathcal{K}$, where \mathcal{K} is the complex conjugation, and it fulfills the relation $T^2 = 1$. Time-reversal symmetry restricts the form of the non-degenerate energy eigenstate as

$$T \begin{pmatrix} \psi_e(x) \\ \psi_h(x) \end{pmatrix} = \begin{pmatrix} \psi_e^*(x) \\ -\psi_h^*(x) \end{pmatrix} = e^{i\varphi} \begin{pmatrix} \psi_e(x) \\ \psi_h(x) \end{pmatrix}, \quad (14)$$

where φ depends on the global phase of the wave function. For concreteness, we fix this global phase such that $\varphi = 0$. Given an eigenstate ψ with an arbitrary global phase, eigenstate with $\varphi = 0$ is obtained as $\psi(x) + T\psi(x)$. This choice $\varphi = 0$ leads to

$$\text{Im}[\psi_e(x)] = 0, \quad (15a)$$

$$\text{Re}[\psi_h(x)] = 0. \quad (15b)$$

Equations (7), (13) and (15) constrain the form of the wave function:

$$\psi(x) = \begin{pmatrix} A_e \{ e^{-\kappa x} \sin(Kx - \phi_e) + p e^{-\kappa(L-x)} \sin[K(L-x) - \phi_e] \} \\ i A_h \{ e^{-\kappa x} \sin(Kx - \phi_h) - p e^{-\kappa(L-x)} \sin[K(L-x) - \phi_h] \} \end{pmatrix}, \quad (16)$$

where A_e and A_h are normalization factors,

$$\phi_e = \arctan \left[\frac{p e^{-\kappa L} \sin(KL)}{1 + p e^{-\kappa L} \cos(KL)} \right], \quad (17a)$$

$$\phi_h = \arctan \left[\frac{-p e^{-\kappa L} \sin(KL)}{1 - p e^{-\kappa L} \cos(KL)} \right] \quad (17b)$$

are phases, and $p = +1$ ($p = -1$) corresponds to the behavior under inversion, that is, to the upper (lower) sign in Eq. (13).

In the limit $L \gg \xi > 1/k_F$, the following approxima-

tions can be made:

$$p = \text{sign} \left[\sin \left(\sqrt{k_F^2 - 1/\xi^2} L \right) \right], \quad (18a)$$

$$\phi_e = -\phi_h = \phi \approx e^{-L/\xi} \left| \sin \left(\sqrt{k_F^2 - 1/\xi^2} L \right) \right|, \quad (18b)$$

$$A_e = A_h = A \approx \frac{1}{\sqrt{\frac{\xi}{2} \left(1 - \frac{\cos(\phi/2)}{k_F^2 \xi^2} \right)}}. \quad (18c)$$

We note that p changes sign where the minigap vanishes.

To obtain Eq. (18a), we compare the wave function in Eqs. (6) and in (16), yielding

$$\phi_e = \arctan \left[\frac{\alpha_1 u_{k_1} + \alpha_2 u_{k_2}}{i(\alpha_2 u_{k_2} - \alpha_1 u_{k_1})} \right]. \quad (19)$$

The coefficient vector $(\alpha_1, \alpha_2, \alpha_3, \alpha_4)^\top$ is the nullspace of the matrix \mathcal{M} , which we find analytically by Gauss elimination. Comparing Eqs. (17a) and (19) up to leading order in $e^{-L/\xi}$, we find Eq. (18a). Furthermore, we find the approximate formula for the phases in Eq. (18b) using Eqs. (17), by taking leading-order approximation in $e^{-L/\xi}$, and utilizing Eq. (18a). To obtain Eq. (18c), we assumed that the electron and hole character of the wave function has exactly equal probability in the limit of $L \gg \xi > 1/k_F$, which results in $A_e = A_h$. We derived Eq. (18c) from the norm of wave function in Eq. (16) by taking the limit for $L \rightarrow \infty$. We will use Eqs. (18) to derive an approximate analytical formula for the dephasing susceptibility to disorder shown in Eq. (29).

B. Standard deviation of the minigap

Now we describe the broadening of the minigap distribution due to on-site disorder. The full Hamiltonian of the disordered system can be written as

$$H_C = \mathcal{H}_C(-i\hbar\partial_x) + H_{\text{dis}}, \quad (20)$$

where $H_{\text{dis}} = \delta\mu_C(x)\sigma_z$ is the disorder Hamiltonian, representing disorder in the chemical potential. We model disorder as a collection of potential steps, where the lengths of the steps are equal and denoted by a_{dis} :

$$\delta\mu_C(x) = \sum_{i=1}^{N_{\text{dis}}} \delta\mu_i^{(C)} \chi_i(x), \quad (21)$$

where

$$\chi_i(x) = \begin{cases} 1 & i-1 \leq x/a_{\text{dis}} < i, \\ 0 & \text{otherwise.} \end{cases} \quad (22)$$

This model is a natural analog of the disorder model we used in the Kitaev chain, with the identification $a = a_{\text{dis}}$, where a is the lattice constant of the Kitaev chain.

We regard disorder as a perturbation, and calculate the first order energy shift. Naively, one should do degenerate perturbation theory, since the antibonding and bonding Majorana energies are close to each other. However, disorder does not couple them, hence non-degenerate perturbation theory is sufficient. The proof of this is as follows.

Due to the particle-hole symmetry of the BdG Hamiltonian: $\langle \psi | H_{\text{dis}} | P\psi \rangle = \langle P\psi | H_{\text{dis}} | \psi \rangle = 0$, where $|\psi\rangle$ and $|P\psi\rangle$ are the positive and negative energy solution of the BdG Hamiltonian, and $P = (\mathbb{1} \otimes \sigma_x)\mathcal{K}$ is the operator of the particle-hole symmetry. This can be seen by

$$\begin{aligned} \langle \psi | H | P\psi \rangle &= -\langle \psi | PH | \psi \rangle = \\ &= -\langle P\psi | H | \psi \rangle^* = -\langle H\psi | P\psi \rangle = -\langle \psi | HP\psi \rangle, \end{aligned} \quad (23)$$

where the first equation is implied by the fact that H anticommutes with P , the second equation is the consequence of the anti-unitary property of P , the third equation is obtained by flipping the scalar product, and the fourth equation is implied by H being Hermitian.

Applying the relation $\langle \psi | H_{\text{dis}} | P\psi \rangle = 0$ to the antibonding $|\psi\rangle$ and bonding $|P\psi\rangle$ Majorana wave functions, we conclude that they are uncoupled and therefore the first-order disorder-induced shift of the signful minigap is $\delta\epsilon_0^{(1)} = \langle \psi | H_{\text{dis}} | \psi \rangle$. Using Eqs. (6) and (21), this shift can be written as

$$\langle \psi | H_{\text{dis}} | \psi \rangle = \sum_{i=1}^{N_{\text{dis}}} \delta\mu_i^{(C)} \zeta_i, \quad (24)$$

where

$$\zeta_i = \int_{(i-1)a_{\text{dis}}}^{ia_{\text{dis}}} \left[|\psi_e(x)|^2 - |\psi_h(x)|^2 \right] dx. \quad (25)$$

In analogy with our disorder model in the Kitaev chain, discussed in section II, we assume independence and normal distribution for the chemical potential disorder, which we denote as $\delta\mu_i^{(C)} \sim \mathcal{N}(0, \sigma_\mu)$, where σ_μ is the disorder strength, and $\delta\mu_i^{(C)}$ -s are independent of each other. From Eq. (24), we conclude that the disorder matrix element also follows Gaussian distribution:

$$\langle \psi | H_{\text{dis}} | \psi \rangle \sim \mathcal{N}(0, \sigma_{\epsilon_0}), \quad (26)$$

where $\sigma_{\epsilon_0} = \sigma_\mu \sqrt{\sum_{j=1}^{N_{\text{dis}}} \zeta_j^2}$ the standard deviation of the distribution of the signful minigap.

Let us suppose that $|\psi_e(x)|^2 - |\psi_h(x)|^2$ varies slowly on the scale of a_{dis} . This implies

$$\begin{aligned} \sum_{i=1}^{N_{\text{dis}}} \zeta_i^2 &\approx \sum_{i=1}^{N_{\text{dis}}} a_{\text{dis}}^2 \left[|\psi_e(ia_{\text{dis}})|^2 - |\psi_h(ia_{\text{dis}})|^2 \right]^2 \\ &\approx a_{\text{dis}} \int_0^L \left[|\psi_e(x)|^2 - |\psi_h(x)|^2 \right]^2 dx. \end{aligned} \quad (27)$$

Therefore, the dephasing susceptibility to disorder is be obtained as

$$\chi \equiv \frac{\sigma_{\epsilon_0}}{\sigma_\mu} = \sqrt{a_{\text{dis}} \int_0^L \left[|\psi_e(x)|^2 - |\psi_h(x)|^2 \right]^2 dx}. \quad (28)$$

By solving Eq. (8) numerically, we obtain the values $\alpha_{i,\text{num}}$ of α_i . Substituting these numerical values $\alpha_{i,\text{num}}$ and $\epsilon_{0,\text{num}}$ into Eqs. (4) and (16), we obtain the semi-analytical wave function $\psi_e(x)$ and $\psi_h(x)$. After normalization, Eq. (28) can be performed. Results, shown in Fig. 4b as 'exact', are discussed below.

As an alternative to the above semi-analytical approach, an approximate analytical formula can be obtained by substituting the form of the wave function in Eqs. (16) into Eq. (28) using Eqs. (18). After the integration over x , and taking series expansion in $\kappa e^{-\kappa L}$, the dephasing susceptibility to disorder in limit of $L \gg \xi > 1/k_F$ can be written as

$$\begin{aligned} \chi &= \sqrt{\frac{a_{\text{dis}}}{2\xi}} e^{-L/\xi} \times \\ &\times \sqrt{\frac{8L}{\xi} - 3 + \left(\frac{4L}{\xi} + 3 \right) \cos \left(2\sqrt{k_F^2 - 1/\xi^2} L \right)}. \end{aligned} \quad (29)$$

Equation (29) is the key result of our work. It reveals that the dephasing susceptibility (and hence the dephasing rate) as a function of system parameters exhibits oscillations that are out-of-phase with the oscillations of the clean minigap given in Eq. (12). This is apparent as Eq. (12) contains a sine whereas Eq. (29) contains a cosine.

Furthermore, Eq. (29) also suggests the absence of dephasing sweet spots in this setting: the long expression below the square root in Eq. (29) is always positive due to the condition $L \gg \xi$.

In conclusion, we have described a semi-analytical procedure, and an approximate analytical procedure, to estimate the disorder-induced broadening of the distribution of the signful minigap in a continuum model of a 1D topological superconductor.

IV. CONNECTING THE CONTINUUM MODEL WITH THE KITAEV CHAIN

The Kitaev chain [Eq. (1)] is a discretized version of the continuum model [Eq. (21)], and vice versa, the continuum model can be obtained from the Kitaev chain via the envelope-function approximation. The relation of the two models is outlined in Ref. 62, but for the sake of self-containedness, we describe it here in detail. We will show, in section IV B, that in fact, our numerical results obtained for the Kitaev chain are consistent with the semi-analytical results obtained for the continuum model. Beforehand, in IV A, we match the parameters of the two models via matching their dispersion relations as shown in Fig. 3.

A. Matching the parameters of the two models

To match the two models, we recall the BdG Hamiltonian of the Kitaev chain in momentum space, which reads

$$\mathcal{H}_K(k) = (-2t \cos(ka) - \mu_K) \sigma_z + 2\Delta_K \sin(ka) \sigma_y. \quad (30)$$

Here we note that the momentum-space superconducting term $2\Delta_K \sin(ka) \sigma_y$ of the Kitaev chain is proportional to σ_y , whereas the corresponding term $\Delta'_C \hbar k \sigma_x$ of the continuum model [Eq. (2)] is proportional to σ_x . This difference is irrelevant, can be transformed away with a unitary transformation in Nambu space, since the rest of both Hamiltonians is proportional to σ_z .

Matching the continuum model and the Kitaev chain model is based on the following criteria:

1. The lengths in the two models are naturally matched as $L = Na$, where L is the length of the wire and N is the number of sites in the lattice model.

2. In the absence of superconductivity, the effective mass in the vicinity of $k = 0$ has to be the same in the two models, which yields the condition:

$$m = \frac{\hbar^2}{2ta^2}. \quad (31a)$$

3. In the absence of the superconducting terms, the minima of the bulk spectra have to be at the same energy. This is achieved by adjusting the chemical potentials in the following way:

$$\mu_C = 2t + \mu_K. \quad (31b)$$

4. The low-energy (close to zero energy) spectra of the two models will be similar if the minimum of the bulk normal band is just slightly below zero energy; formally this can be written as

$$0 < 1 + \frac{\mu_K}{2t} \ll 1. \quad (31c)$$

5. In the presence of superconductivity, the superconducting gaps have to be equal, a condition approximately satisfied by the identification

$$\Delta'_C = \frac{\Delta_K a}{\hbar} \sqrt{2 - \frac{\mu_K}{t}}. \quad (31d)$$

We note that here we have already assumed that Eqs. (31a) and (31b) are fulfilled. Eq. (31d) is an approximation in the sense that we match energy gaps of the two models that are opened at k_F , i.e., at the wave number where the band touches zero in the absence of the superconductivity. The actual gap (i.e., the energy difference minimized over the wave number) is in general located at a slightly different wave number k_0 , but in the limit of Eq. (31c), $k_0 \approx k_F$.

Based on the above criteria, we choose the parameter values listed in Table I to compare the results of the Kitaev chain and the continuum model.

The energy dispersion of the Kitaev chain (blue solid) and that of the continuum model (red dashed) are compared over the 1D Brillouin zone in Fig. 3a, and in the vicinity of the Brillouin zone center and the Fermi wave number in Fig. 3b.

Below, we will need the following relations between the parameters of the two models:

$$k_F = \frac{\sqrt{2 + \frac{\mu_K}{t}}}{a}, \quad (32a)$$

$$\Delta_C = \Delta_K \sqrt{4 - \left(\frac{\mu_K}{t}\right)^2}, \quad (32b)$$

$$\xi = \frac{2ta}{\Delta_K \sqrt{2 - \frac{\mu_K}{t}}}. \quad (32c)$$

We obtain Eq. (32a) from Eq. (3a) by substituting Eqs. (31a) and (31b). We get Eq. (32b) from Eq. (3c) by substituting Eqs. (31d) and (32a). We obtain Eq. (32c) from Eq. (3d) by combining Eqs. (3b), (31a), (3a) and (3c).

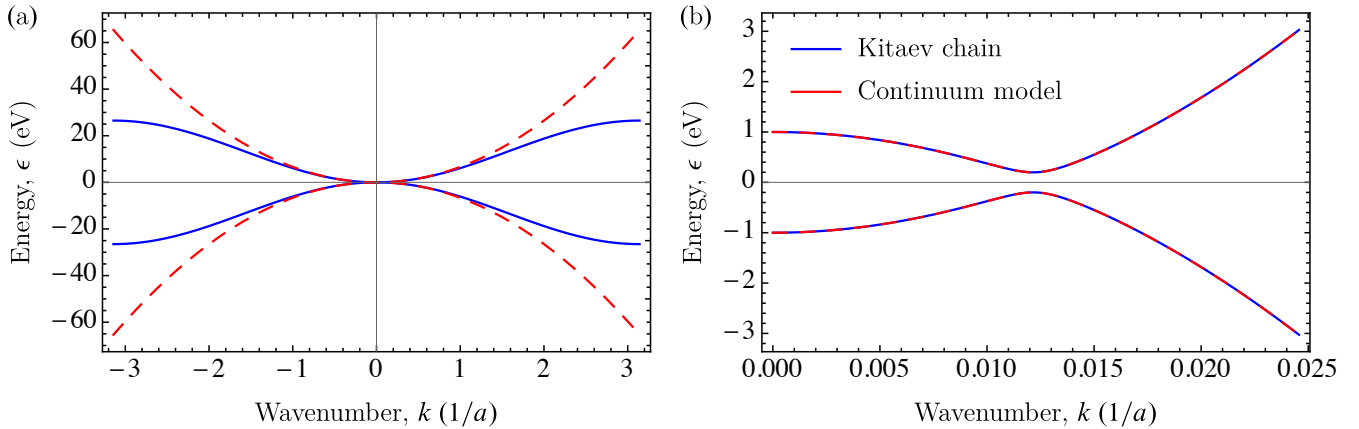


FIG. 3. The Kitaev chain band structure (blue) and the continuum model band structure (red), (a) over the 1D Brillouin zone, (b) in the vicinity of zero energy, with parameters chosen such that the band structures match each other in the vicinity of zero energy. See Table I for parameter values.

B. Comparing the results of the two models

Here, we show the correspondence of the Kitaev chain and continuum model results for the minigap ε_0 , the disorder-induced standard deviation σ_{ε_0} , and the dephasing susceptibility χ .

In Fig. 4a, we plot the minigap of the clean system as a function of the chain length. Red points show the numerical result from the Kitaev chain model, whereas the red solid line shows the semi-analytical exact result from the continuum model, obtained by solving Eq. (10) numerically. Dashed green line shows the result of the Eq. (12a). Parameter values are those listed in Table I. In Fig. 4a, the Kitaev chain result (red points) and the exact result from the continuum model (red solid line) are indistinguishable. The analytical approximate result (green dashed line) shows a slight deviation from the other two data sets for short chain, but becomes indistinguishable from those for long chains.

In Fig. 4b, we plot the dephasing susceptibility, that is, the ratio of minigap standard deviation σ_{ε_0} and the disorder strength σ_μ , as the function of the chain length. The Kitaev model result (points) is obtained numerically, using 10000 random disorder realizations for each length. Here again, the two models show satisfactory agreement.

V. SIGNFUL MINIGAP DISTRIBUTION AND MAJORANA QUBIT DEPHASING

In this section, we complete our primary task, and describe the dephasing dynamics of a Majorana qubit subject to quasistatic disorder.

Consider a Majorana qubit encoded in two identical topological superconducting wires. All parameters are assumed to be equal, including the disorder strength. The two wires are assumed to be decoupled from each other (no tunneling between the two wires). Restrict our

attention to the globally even ground state of this setup, which is spanned by the basis states $|0\rangle \equiv |e_1, e_2\rangle$ and $|1\rangle \equiv |o_1, o_2\rangle$, where the names e and o refer to the even and odd fermion parities of the corresponding states, and the indices 1 and 2 refer to the first and second wire, respectively.

To perform a qubit dephasing experiment, one usually creates an initial state $|\psi_i\rangle$ that is a balanced superposition of the two basis states, e.g., with a qubit polarization vector along the x direction

$$|\psi_i\rangle = \frac{1}{\sqrt{2}} (|0\rangle + |1\rangle). \quad (33)$$

The qubit polarization vector (Bloch vector) for this state is

$$\vec{p} \equiv \langle \psi_i | \vec{\sigma} | \psi_i \rangle = (1, 0, 0), \quad (34)$$

where $\vec{\sigma} = (\sigma_x, \sigma_y, \sigma_z)$ is the vector of Pauli matrices. Note that the preparation of this initial state itself can be corrupted by disorder, a complication that we disregard here.

After preparation, the relative phase between the two basis states evolves in time due to the excess energy $\epsilon_0^{(1)}$ of o_1 with respect to e_1 in wire 1, and the excess energy $\epsilon_0^{(2)}$ of o_2 with respect to e_2 in wire 2. In particular, the time-dependent wave function, up to an irrelevant global phase, reads

$$|\psi(t)\rangle = \frac{1}{\sqrt{2}} \left(|0\rangle + e^{-i(\epsilon_0^{(1)} + \epsilon_0^{(2)})t/\hbar} |1\rangle \right). \quad (35)$$

Then, the quasistatic assumption implies that on average, for a large number of measurements, the qubit po-

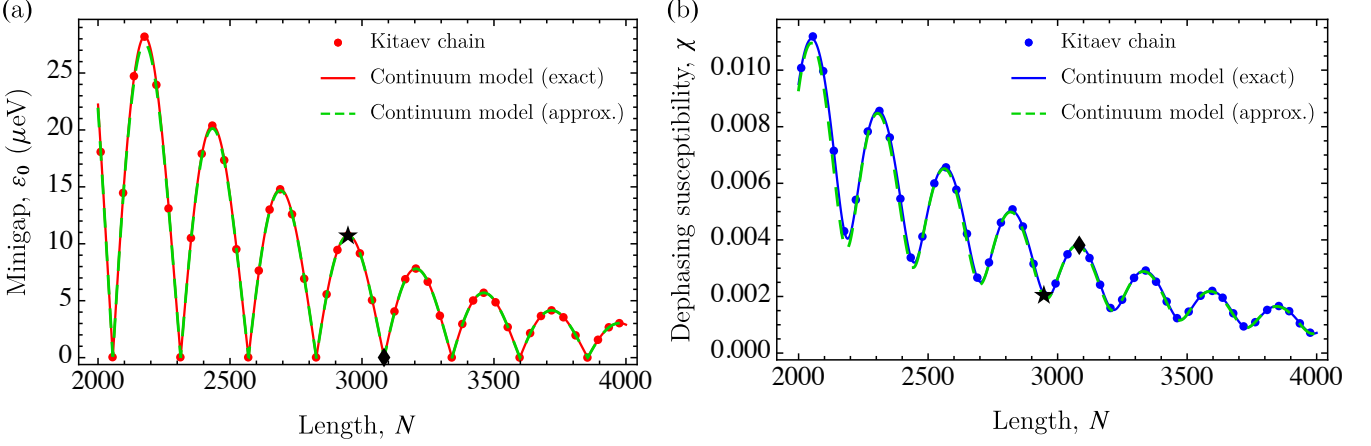


FIG. 4. Comparison of continuum-model (lines) and Kitaev-model (dots) results for the minigap and its standard deviation. (a) Minigap as a function of length for the clean system. (b) Dephasing susceptibility to disorder – that is, the ratio $\chi = \sigma_{\epsilon_0}/\sigma_\mu$ of the standard deviation of the minigap and the strength of the on-site disorder – is shown as a function of the length. See Table I for parameter values. In both panels, star and diamond denote two specific chain lengths, for which the dephasing curves are shown in Fig. 5.

larization vector evolves in time as

$$\langle \vec{p}(t) \rangle \equiv \langle \psi(t) | \vec{\sigma} | \psi(t) \rangle = \int d\epsilon \rho(\epsilon) \begin{pmatrix} \cos(\epsilon t/\hbar) \\ -\sin(\epsilon t/\hbar) \\ 0 \end{pmatrix}, \quad (36)$$

where $\epsilon = \epsilon_0^{(1)} + \epsilon_0^{(2)}$ is the random qubit energy splitting, and $\rho(\epsilon)$ is its pdf.

We illustrate the dephasing dynamics by calculating $\langle p_x(t) \rangle$, the x component of the disorder-averaged polarization vector as the function of time. We will refer to this function as the *dephasing curve*. We evaluate the dephasing curve based on the observation that the signful minigap has a Gaussian pdf in the parameter range we consider. Based on Eq. (36), this implies the following well-known result^{58,65} for the dephasing curve:

$$\langle p_x(t) \rangle = e^{-\left(\frac{\sigma_{\epsilon_0}}{\hbar} t\right)^2} \cos\left(\frac{2\epsilon_{0,c}}{\hbar} t\right), \quad (37)$$

where $\epsilon_{0,c}$ is the clean minigap. This result implies that dephasing follows Gaussian decay, and this decay is characterized by the time scale

$$T_2^* = \frac{\hbar}{\sigma_{\epsilon_0}} = \frac{\hbar}{\sigma_\mu \chi}, \quad (38)$$

which is often called the *inhomogeneous dephasing time*.

Fig. 5a shows two dephasing curves for the parameter set shown in Table I, the solid line showing fast oscillations, and the dashed line showing no oscillations. The dashed line corresponds to the diamond ($N = 3083$) in Fig. 4, with chain length fine-tuned such that the clean minigap vanishes. The solid line corresponds to the star

($N = 2947$) in Fig. 4, with chain length fine-tuned such that the clean minigap has a local maximum. For both chain lengths, the pdf of the signful minigap is Gaussian. However, the mean of the signful minigap (which is the same as the clean minigap $\epsilon_{0,c}$) is zero for the $N = 3083$ case, and finite for the $N = 2947$ case, the latter being responsible for the oscillations in Fig. 5a. This figure also illustrates the out-of-phase relation between the clean minigap and dephasing susceptibility (see, e.g., Fig. 2)b: the smaller the clean minigap, the faster the dephasing.

It is also interesting to note that the oscillation (Larmor precession) induced by the finite clean minigap, as shown by the solid line in Fig. 5a, has a much smaller time scale than the dephasing time. It would be interesting to study in detail how this fast Larmor precession influences the fidelity of quantum gates, e.g., based on braiding of MZMs²¹.

Fig. 5b shows the inhomogeneous dephasing time as a function of the length for longer chains. The dephasing time is calculated analytically by substituting the approximate formula of χ given by Eq. (29) into Eq. (38). Aside from the oscillations seen in Fig. 5b, the dependence of the dephasing time on the chain length is dominated by an exponential factor. The figure corresponds to a disorder strength $\sigma_\mu = 2.8 \mu\text{eV}$, which corresponds to the dephasing time $T_2^* = 200 \text{ ns}$ for $L/\xi = 5$.

The inset of Fig. 5b shows the calculated inhomogeneous dephasing time values for specific chain lengths. We use this table, in particular the inhomogeneous dephasing time value $T_2^* = 200 \text{ ns}$ at $L/\xi = 5$, to relate our results to the earlier dephasing-time estimates of Ref. 35 (see Table I therein). Ref. 35 predicts this T_2^* value from intrinsic sources, without any disorder in the sample. Therefore, our parameter value $\sigma_\mu = 2.8 \mu\text{eV}$ provides an estimate for the crossover disorder strength,

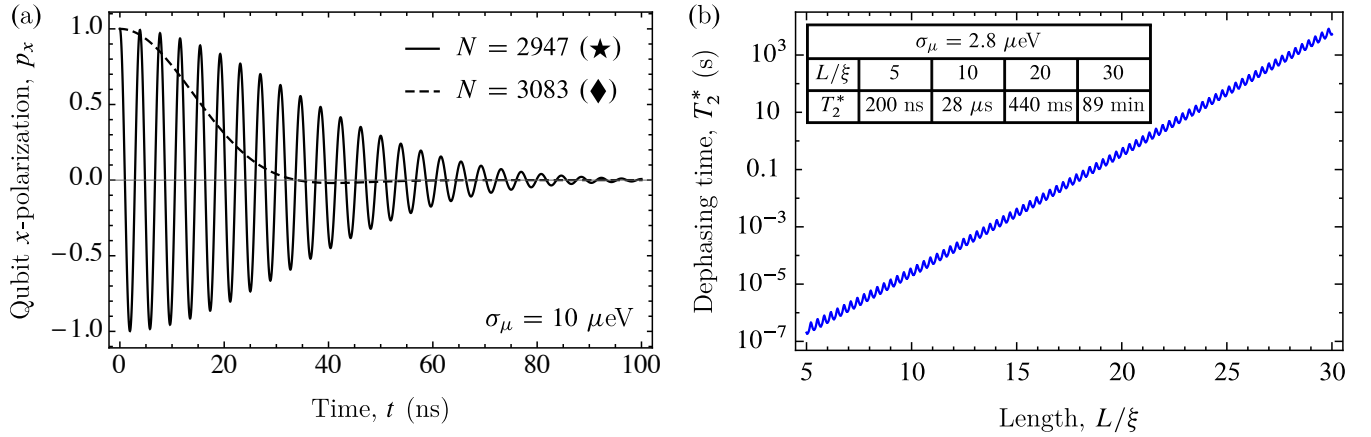


FIG. 5. Dephasing of a Majorana qubit due to quasistatic disorder. (a) Dephasing curves. The x component of the disorder-averaged polarization vector as a function of time for two different lengths (see star and diamond in Fig. 4.) The envelopes of the curves follows Gaussian dephasing. The finiteness of the mean of the signful minigap is responsible for the oscillations of the solid line. The out-of-phase oscillation between the clean minigap and dephasing susceptibility is illustrated: the longer chain (dashed line) has faster dephasing according to it has smaller clean minigap. (b) Inhomogeneous dephasing time as a function of the length for disorder strength $\sigma_\mu = 2.8 \mu\text{eV}$. Table inset shows the same for specific lengths.

that is, the disorder strength above which dephasing due to quasi-static disorder dominates the intrinsic dephasing mechanisms of a clean system (homogeneous $1/f$ charge noise, phonons, equilibrium quasiparticles).

Experimental data indicates that the typical energy scale of local electrostatic fluctuations in state-of-the-art semiconductor quantum devices is of the order of a few μeV -s, see, e.g., Table II of Ref. 35. This suggests that the mechanism we describe here will be relevant for early-stage Majorana-qubit experiments.

VI. DISCUSSION

In the main part of this work, we used a model of short-range-correlated disorder. This is admittedly a minimal model of disorder in real samples, nevertheless we find it important and relevant to provide the corresponding results, because (i) this is a conceptually simple, canonical model, often used in the literature, applied to effects ranging from Anderson localisation to Majorana physics^{29,42}, and (ii) these results also serve as benchmark for more realistic models. Also, the level of disorder in state-of-the-art hybrid nanowires seems to be too strong to allow for the clear observation of Majorana zero modes, which suggest that disorder will likely play a dominant role also in the initial Majorana-qubit experiments, e.g., qubit dephasing time measurements. In real nanowire samples, disorder might arise due to various physical mechanisms⁶⁶, e.g., fluctuating charge traps in the substrate, atoms, ions, molecules contaminating the wire surface, impurity atoms built in to the crystal upon growth, electron scattering on rough or oxidized wire surface and core-shell interface, inhomogeneous strain patters due to thermal expansion coefficient

mismatch and metal deposition (shell, gates, contacts), gate-voltage fluctuations, etc. It is an important ongoing effort to mitigate these mechanisms; alternatively, it is useful to characterize and control their effects on Majorana qubit decoherence.

In our dephasing calculation, we have chosen the quasistatic approximation also for its conceptual simplicity and widespread use in the literature^{49,51}. In real devices, classical or quantum noise often follows a characteristic noise spectrum, e.g., $1/f$ noise^{35,40,46,47,55–57,67–69}, Johnson-Nyquist noise, quantum noise of phonons^{35,36}, gate-voltage fluctuations^{31,35,39,40}, etc. Going beyond the quasistatic approximation by incorporating these frequency-dependent noise features would be an important addition to this work. An especially appealing task is to describe the combined effect of static spatial disorder and fluctuating electric fields; this direction might actually reveal connections between actual device physics and the minimal model used in our present work. A conceptually different, but equally important information loss mechanism for Majorana qubits is quasiparticle poisoning^{27,32,33,70–72}.

In this work, we focused on the case of low disorder, in the hope that material growth and device fabrication advances will convey qubit experiments in that parameter range. Current devices might have much stronger disorder^{73–75} and it is an interesting extension of our work to study how Majorana qubit dephasing occurs in the presence of strong disorder. A further natural extension of our work is to step-by-step move from the Kitaev-chain minimal model to more realistic real-space models, e.g., from 1D Rashba wire^{1,2,76} to 3D Schrödinger-Poisson models^{75,77,78}, and beyond.

VII. CONCLUSIONS

We have studied the Majorana minigap of the disordered topological Kitaev chain, serving as a minimal model of dephasing of Majorana qubits. We characterized the Gaussian probability distributions of the signful minigap, using numerics as well as simple semi-analytical and approximate analytical techniques. In the parameter range we studied, we established a Gaussian decay envelope for the dephasing curve, as a consequence of the Gaussian distribution of the signful minigap. We have found that the standard deviation of the signful minigap, and hence the dephasing rate, oscillates as the function of system parameters out-of-phase with respect to the oscillations of the clean minigap. We have also pointed out the absence of dephasing sweet spots in our dephasing model of quasistatic disorder. We expect that our results will be used in the design and interpretation of future experiments, aiming to demonstrate topologically protected quantum memory, quantum dynamics, or quantum computing, based on Majorana zero modes.

ACKNOWLEDGMENTS

We thank J. Asbóth, P. Brouwer, L. Oroszlány, A. Romito, and G. Széchenyi for helpful discussions, and G. Takács for computational resources. This research was supported by the Ministry of Innovation and Technology and the National Research, Development and Innovation Office (NKFIH) within the Quantum Information National Laboratory of Hungary, the BME Nanotechnology and Materials Science TKP2020 IE grant (BME IE-NAT TKP2020), the Quantum Technology National Excellence Program (Project No. 2017-1.2.1-NKP-2017-00001), and the OTKA Grants FK124723 and FK132146.

Appendix A: Inferring the standard deviation of the signful minigap from samples of the minigap

Figure 2b shows the standard deviation of σ_{ϵ_0} of the signful minigap ϵ_0 of a Kitaev chain due to disorder. How did we compute σ_{ϵ_0} ? The smallest non-negative eigenvalue of the BdG matrix is the *absolute value* of the signful minigap, hence its standard deviation taken over many disorder realizations does not provide σ_{ϵ_0} . Here, we provide an indirect way to compute σ_{ϵ_0} by assuming that the signful minigap is normally distributed, an assumption in accordance with our result (26). Under that assumption, the absolute value of the signful minigap has *folded normal distribution*. We have an easy access to samples of the minigap by using BdG Hamiltonian, and by following the procedure outlined below, we are able to compute σ_{ϵ_0} from samples of the minigap.

Let us use a general notation for easier readability. The probability density function of the normal random vari-

able X , representing the signful minigap, reads

$$f_X(x) = \frac{1}{\sqrt{2\pi}\sigma} e^{-\frac{(x-m)^2}{2\sigma^2}}, \quad (A1)$$

where m is the mean and σ is the standard deviation of X . The probability density function of the random variable $|X|$, representing the minigap, is

$$f_{|X|}(x) = \frac{1}{\sqrt{2\pi}\sigma} e^{-\frac{(x-m)^2}{2\sigma^2}} \left(1 + e^{\frac{2mx}{\sigma^2}}\right), \quad (A2)$$

which is often called a folded normal distribution.

We estimate the parameters m and σ (mean and standard deviation of signful minigap) from a sample $\{x_i | i = 1, \dots, n\}$ of $|X|$ (the minigap). Here n is the size of the sample. Our estimation is based on the maximum likelihood estimation procedure. The log-likelihood of the distribution estimated from the sample $\{x_i\}$ can be written as

$$\begin{aligned} l(\{x_i\}; m, \sigma) = & \log \left[\prod_{i=1}^n f_{|X|}(x_i) \right] = \\ & -\frac{n}{2} \log(2\pi\sigma^2) - \sum_{i=1}^n \frac{(x_i - m)^2}{2\sigma^2} \\ & + \sum_{i=1}^N \log \left(1 + e^{\frac{2mx_i}{\sigma^2}} \right). \end{aligned} \quad (A3)$$

To estimate the value of m and σ , we need to find the maximum point of the likelihood function, hence we take $\partial_m l(\{x_i\}; m, \sigma) = 0$ and $\partial_\sigma l(\{x_i\}; m, \sigma) = 0$, that lead to

$$m = \frac{1}{n} \sum_{i=1}^n x_i \tanh \left(\frac{mx_i}{\sigma} \right), \quad (A4a)$$

$$\sigma^2 = m^2 + \frac{1}{n} \sum_{i=1}^n x_i^2 - \frac{2m}{n} \sum_{i=1}^n x_i \tanh \left(\frac{mx_i}{\sigma} \right). \quad (A4b)$$

From Eqs. (A4a) and (A4b), we get

$$\sigma^2 = \left(\frac{1}{n} \sum_{i=1}^n x_i^2 \right) - m^2. \quad (A5)$$

In general, the coupled Eqs. (A4a) and (A4b) have to be solved. However, in our case, to determine the standard deviation of the signful minigap, Eq. (A5), is sufficient as know the square of the signful minigap mean m : it is equal to the square of the minigap of the clean system $\varepsilon_{0,c}$. This implies the formula

$$\sigma_{\epsilon_0} = \sqrt{\left(\frac{1}{n} \sum_{i=1}^n \varepsilon_{0,i}^2 \right) - \varepsilon_{0,c}^2}, \quad (A6)$$

where $\varepsilon_{0,i}$ s are minigaps in disordered realizations and $\varepsilon_{0,c}$ is the minigap for the clean system. We used this result to compute the data in Fig. 2b.

Appendix B: Comparison with the results of Brouwer et al. PRL 2011

In the main text, we predict a normal distribution for signful minigap ϵ_0 . On the other hand, the key result of Ref. 29 is that the *minigap envelope* $\varepsilon_{0,\max}$ (for clarification, see their Fig. 1c) has a log-normal distribution. Although the two quantities (signful minigap and minigap envelope) are not the same, they are in fact interrelated. In this appendix, we identify a parameter range where both our results and the results of Ref. 29 are valid, and establish the relation of these results. Our comparison suggests that the two unknown constants appearing in the analytical results of Ref. 29 (C_m and C_v , see below) are actually zero.

The main result of Ref. 29 is as follows. The quantity $\ln(\varepsilon_{0,\max}/2\Delta_C)$ has a normal distribution with mean and variance given by their Eq. (16), that is,

$$\langle \ln(\varepsilon_{0,\max}/2\Delta_C) \rangle = -L[1/\xi - 1/2l] + C_m, \quad (B1a)$$

$$\text{var} \ln(\varepsilon_{0,\max}/2\Delta_C) = L/2l + C_v. \quad (B1b)$$

Here, C_m and C_v are the unknown constants, that is, unknown order-of-unity corrections independent of L , l and ξ . Furthermore, $l = \hbar^2 v_F^2 / \gamma$ is the mean free path, where γ corresponds to the disorder strength in their model, which is identified with our model as $\gamma = a_{\text{dis}}\sigma_\mu^2$.

Their results stand if the following conditions are satisfied:

$$1/k_F \ll \xi, \quad (B2a)$$

$$\xi < 2l, \quad (B2b)$$

$$\varepsilon_{0,\max} \ll \min(\Delta_C, \hbar/\tau), \quad (B2c)$$

where $\tau = \hbar v_F / l$. On the other hand, our result for the clean minigap (12) is valid if $L \gg \xi$, and our result for the dephasing susceptibility to disorder (29) is valid if $L \gg \xi$ and if disorder is weak.

First, we assume that the parameter range of validity of the two results have some overlap, and show that in such a common parameter range, the two results are consistent. Second, we provide an example for the common parameter range where both results should be valid and hence should be consistent with each other.

To show the consistency of the two results, we suppose that

$$l \gg \xi, \quad (B3a)$$

$$L/2l \ll 1, \quad (B3b)$$

$$C_m = 0, \quad (B3c)$$

$$C_v = 0. \quad (B3d)$$

Eq. (B3a) stands for weak disorder, whereas Eq. (B3b) together with Eq. (B3d) provides that $\ln(\varepsilon_{0,\max}/2\Delta_C)$ has a standard deviation much smaller than one. Furthermore, the choice of C_m and C_v in Eqs. (B3c-d) is required to match the result of Ref. 29 with our results.

Our results, together with Eqs. (B3) imply that the minigap envelope $\varepsilon_{0,\max}$ approximately follows normal distribution with mean and standard deviation as follows:

$$\langle \varepsilon_{0,\max} \rangle = 2\Delta_C e^{-L/\xi}, \quad (B4a)$$

$$\sigma_{\varepsilon_{0,\max}} = \Delta_C \sqrt{\frac{2L}{l}} e^{-L/\xi} = \sigma_\mu \frac{\sqrt{2L a_{\text{dis}}}}{\xi} e^{-L/\xi}. \quad (B4b)$$

We obtained Eq. (B4a), from Eq. (12a) by taking the limit $k_F \ll 1/\xi$ and by omitting the sinusoidal oscillatory part in the latter. Furthermore, we obtained Eq. (B4b) from Eq. (29) by taking the limit $L \gg \xi$, and by substituting the cosine term with -1 . The latter substitution is needed because the disorder-induced standard deviation of the minigap has a local minimum whenever the clean minigap has a local maximum (see Fig. 4a).

The key mathematical statement we use to show the consistency of Eq. (B1) and Eq. (B4) is the following: If X is a log-normal random variable such that $\ln X$ is a normal random variable with mean μ and standard deviation σ (that is, $\ln X \sim \mathcal{N}(\mu, \sigma)$), and the standard deviation fulfills $\sigma \ll 1$, then X is approximately a normal random variable with mean e^μ and standard deviation $e^\mu \sigma$ (that is, $X \sim \mathcal{N}(e^\mu, e^\mu \sigma)$). This follows from the fact that the exponential function can be well approximated around any point by its linear series expansion in a sufficiently small environment of the point. We apply this approximation to Eq. (B1) using the assumptions of Eq. (B3). This procedure yields Eq. (B4), implying that our result is consistent with the earlier result.

Finally, we provide an example for the common parameter range where both results are valid. Equation (B2a) is satisfied for the parameter set in Table I. In the weak disorder limit, Eq. (B2b) is fulfilled. For weak disorder $\hbar/\tau \ll \Delta_C$, furthermore using Eq. (B4a), the condition $\varepsilon_{0,\max} \ll \hbar/\tau$ is equivalent to the condition

$$\ln(2l/\xi) \ll L/\xi. \quad (B5)$$

In addition, Eq. (B5) and Eq. (B3d) can be combined as

$$\ln(2l/\xi) \ll L/\xi \ll 2l/\xi. \quad (B6)$$

For weak disorder, there is a finite interval for the system length L where Eq. (B6) is fulfilled. For example, for the parameter values given in Table I, and for disorder strength $\sigma_\mu = 10 \mu\text{eV}$, Eq. (B6) is evaluated

$$14500 \ll L/a \ll 4.32 \times 10^{10}. \quad (B7)$$

Note that our numerical results shown in the main text correspond to system lengths that are one order of magnitude smaller than the lower end of this interval.

To conclude, we have established the consistency between the earlier analytical results of Ref. 29 for the statistics of the minigap envelope, and our analytical results for the statistics of the signful minigap described in

the main text. To ensure this consistency, we had to assume that the order-of-unity constant offset parameters

C_m and C_v , which were not calculated in Ref. 29, are actually zero. This indirect determination of the offset parameters is a useful byproduct of the comparison.

¹ Yuval Oreg, Gil Refael, and Felix von Oppen, “Helical liquids and Majorana bound states in quantum wires,” *Phys. Rev. Lett.* **105**, 177002 (2010).

² Roman M. Lutchyn, Jay D. Sau, and S. Das Sarma, “Majorana fermions and a topological phase transition in semiconductor-superconductor heterostructures,” *Phys. Rev. Lett.* **105**, 077001 (2010).

³ Jay D. Sau, Sumanta Tewari, Roman M. Lutchyn, Tudor D. Stanescu, and S. Das Sarma, “Non-Abelian quantum order in spin-orbit-coupled semiconductors: Search for topological Majorana particles in solid-state systems,” *Phys. Rev. B* **82**, 214509 (2010).

⁴ V. Mourik, K. Zuo, S. M. Frolov, S. R. Plissard, E. P. A. M. Bakkers, and L. P. Kouwenhoven, “Signatures of Majorana fermions in hybrid superconductor-semiconductor nanowire devices,” *Science* **336**, 1003–1007 (2012).

⁵ Elsa Prada, Pablo San-Jose, Michiel W. A. de Moor, Attila Geresdi, Eduardo J. H. Lee, Jelena Klinovaja, Daniel Loss, Jesper Nygård, Ramón Aguado, and Leo P. Kouwenhoven, “From Andreev to Majorana bound states in hybrid superconductor–semiconductor nanowires,” *Nature Reviews Physics* **2**, 575–594 (2020).

⁶ Anindya Das, Yuval Ronen, Yonatan Most, Yuval Oreg, Moty Heiblum, and Hadas Shtrikman, “Zero-bias peaks and splitting in an al–inas nanowire topological superconductor as a signature of majorana fermions,” *Nature Physics* **8**, 887–895 (2012).

⁷ M. T. Deng, C. L. Yu, G. Y. Huang, M. Larsson, P. Caroff, and H. Q. Xu, “Anomalous zero-bias conductance peak in a nb–insb nanowire–nb hybrid device,” *Nano Letters* **12**, 6414–6419 (2012).

⁸ A. D. K. Finck, D. J. Van Harlingen, P. K. Mohseni, K. Jung, and X. Li, “Anomalous modulation of a zero-bias peak in a hybrid nanowire-superconductor device,” *Phys. Rev. Lett.* **110**, 126406 (2013).

⁹ H. O. H. Churchill, V. Fatemi, K. Grove-Rasmussen, M. T. Deng, P. Caroff, H. Q. Xu, and C. M. Marcus, “Superconductor-nanowire devices from tunneling to the multichannel regime: Zero-bias oscillations and magnetoconductance crossover,” *Phys. Rev. B* **87**, 241401 (2013).

¹⁰ M. T. Deng, C. L. Yu, G. Y. Huang, M. Larsson, P. Caroff, and H. Q. Xu, “Parity independence of the zero-bias conductance peak in a nanowire based topological superconductor-quantum dot hybrid device,” *Scientific Reports* **4**, 7261 (2014).

¹¹ S. M. Albrecht, A. P. Higginbotham, M. Madsen, F. Kuemmeth, T. S. Jespersen, J. Nygård, P. Krogstrup, and C. M. Marcus, “Exponential protection of zero modes in majorana islands,” *Nature* **531**, 206–209 (2016).

¹² D. Sherman, J. S. Yodh, S. M. Albrecht, J. Nygård, P. Krogstrup, and C. M. Marcus, “Normal, superconducting and topological regimes of hybrid double quantum dots,” *Nature Nanotechnology* **12**, 212–217 (2017).

¹³ M. T. Deng, S. Vaitiekėnas, E. B. Hansen, J. Danon, M. Leijnse, K. Flensberg, J. Nygård, P. Krogstrup, and C. M. Marcus, “Majorana bound state in a coupled quantum-dot hybrid-nanowire system,” *Science* **354**, 1557–1562 (2016).

¹⁴ H. J. Suominen, M. Kjaergaard, A. R. Hamilton, J. Shabani, C. J. Palmstrøm, C. M. Marcus, and F. Nichele, “Zero-energy modes from coalescing andreev states in a two-dimensional semiconductor-superconductor hybrid platform,” *Phys. Rev. Lett.* **119**, 176805 (2017).

¹⁵ Fabrizio Nichele, Asbjørn C. C. Drachmann, Alexander M. Whiticar, Eoin C. T. O’Farrell, Henri J. Suominen, Antonio Fornieri, Tian Wang, Geoffrey C. Gardner, Candice Thomas, Anthony T. Hatke, Peter Krogstrup, Michael J. Manfra, Karsten Flensberg, and Charles M. Marcus, “Scaling of majorana zero-bias conductance peaks,” *Phys. Rev. Lett.* **119**, 136803 (2017).

¹⁶ Önder Gür, Hao Zhang, Jouri D. S. Bommer, Michiel W. A. de Moor, Diana Car, Sébastien R. Plissard, Erik P. A. M. Bakkers, Attila Geresdi, Kenji Watanabe, Takashi Taniguchi, and Leo P. Kouwenhoven, “Ballistic majorana nanowire devices,” *Nature Nanotechnology* **13**, 192–197 (2018).

¹⁷ M.-T. Deng, S. Vaitiekėnas, E. Prada, P. San-Jose, J. Nygård, P. Krogstrup, R. Aguado, and C. M. Marcus, “Nonlocality of majorana modes in hybrid nanowires,” *Phys. Rev. B* **98**, 085125 (2018).

¹⁸ Anna Grivnin, Ella Bor, Moty Heiblum, Yuval Oreg, and Hadas Shtrikman, “Concomitant opening of a bulk-gap with an emerging possible majorana zero mode,” *Nature Communications* **10**, 1940 (2019).

¹⁹ S. Vaitiekėnas, G. W. Winkler, B. van Heck, T. Karzig, M.-T. Deng, K. Flensberg, L. I. Glazman, C. Nayak, P. Krogstrup, R. M. Lutchyn, and C. M. Marcus, “Flux-induced topological superconductivity in full-shell nanowires,” *Science* **367** (2020), 10.1126/science.aav3392.

²⁰ S. Vaitiekėnas, Y. Liu, P. Krogstrup, and C. M. Marcus, “Zero-bias peaks at zero magnetic field in ferromagnetic hybrid nanowires,” *Nature Physics* **17**, 43–47 (2021).

²¹ Jason Alicea, Yuval Oreg, Gil Refael, Felix von Oppen, and Matthew P. A. Fisher, “Non-Abelian statistics and topological quantum information processing in 1D wire networks,” *Nature Physics* **7**, 412–417 (2011).

²² Jason Alicea, “New directions in the pursuit of Majorana fermions in solid state systems,” *Reports on Progress in Physics* **75**, 076501 (2012).

²³ F Hassler, A R Akhmerov, and C W J Beenakker, “The top-transmon: a hybrid superconducting qubit for parity-protected quantum computation,” *New Journal of Physics* **13**, 095004 (2011).

²⁴ B van Heck, A R Akhmerov, F Hassler, M Burrello, and C W J Beenakker, “Coulomb-assisted braiding of Majorana fermions in a Josephson junction array,” *New Journal of Physics* **14**, 035019 (2012).

²⁵ T. Hyart, B. van Heck, I. C. Fulga, M. Burrello, A. R. Akhmerov, and C. W. J. Beenakker, “Flux-controlled quantum computation with Majorana fermions,” *Phys. Rev. B* **88**, 035121 (2013).

²⁶ David Aasen, Michael Hell, Ryan V. Mishmash, An-

drew Higginbotham, Jeroen Danon, Martin Leijnse, Thomas S. Jespersen, Joshua A. Folk, Charles M. Marcus, Karsten Flensberg, and Jason Alicea, "Milestones toward Majorana-based quantum computing," *Phys. Rev. X* **6**, 031016 (2016).

²⁷ Torsten Karzig, Christina Knapp, Roman M. Lutchyn, Parsa Bonderson, Matthew B. Hastings, Chetan Nayak, Jason Alicea, Karsten Flensberg, Stephan Plugge, Yuval Oreg, Charles M. Marcus, and Michael H. Freedman, "Scalable designs for quasiparticle-poisoning-protected topological quantum computation with Majorana zero modes," *Phys. Rev. B* **95**, 235305 (2017).

²⁸ C. Tutschku, R. W. Reinthalter, C. Lei, A. H. MacDonald, and E. M. Hankiewicz, "Majorana-based quantum computing in nanowire devices," *Phys. Rev. B* **102**, 125407 (2020).

²⁹ Piet W. Brouwer, Mathias Duckheim, Alessandro Romito, and Felix von Oppen, "Probability distribution of Majorana end-state energies in disordered wires," *Phys. Rev. Lett.* **107**, 196804 (2011).

³⁰ G. Goldstein and C. Chamon, "Decay rates for topological memories encoded with Majorana fermions," *Phys. Rev. B* **84**, 205109 (2011).

³¹ Manuel J. Schmidt, Diego Rainis, and Daniel Loss, "Decoherence of Majorana qubits by noisy gates," *Phys. Rev. B* **86**, 085414 (2012).

³² Jan Carl Budich, Stefan Walter, and Björn Trauzettel, "Failure of protection of Majorana based qubits against decoherence," *Phys. Rev. B* **85**, 121405 (2012).

³³ Diego Rainis and Daniel Loss, "Majorana qubit decoherence by quasiparticle poisoning," *Phys. Rev. B* **85**, 174533 (2012).

³⁴ Fabio L. Pedrocchi and David P. DiVincenzo, "Majorana braiding with thermal noise," *Phys. Rev. Lett.* **115**, 120402 (2015).

³⁵ Christina Knapp, Torsten Karzig, Roman M. Lutchyn, and Chetan Nayak, "Dephasing of Majorana-based qubits," *Phys. Rev. B* **97**, 125404 (2018).

³⁶ Pavel P. Aseev, Jelena Klinovaja, and Daniel Loss, "Lifetime of Majorana qubits in Rashba nanowires with nonuniform chemical potential," *Phys. Rev. B* **98**, 155414 (2018).

³⁷ Bela Bauer, Torsten Karzig, Ryan V. Mishmash, Andrei E. Antipov, and Jason Alicea, "Dynamics of Majorana-based qubits operated with an array of tunable gates," *SciPost Phys.* **5**, 4 (2018).

³⁸ Hon-Lam Lai, Pei-Yun Yang, Yu-Wei Huang, and Wei-Min Zhang, "Exact master equation and non-markovian decoherence dynamics of Majorana zero modes under gate-induced charge fluctuations," *Phys. Rev. B* **97**, 054508 (2018).

³⁹ Pavel P. Aseev, Pasquale Marra, Peter Stano, Jelena Klinovaja, and Daniel Loss, "Degeneracy lifting of Majorana bound states due to electron-phonon interactions," *Phys. Rev. B* **99**, 205435 (2019).

⁴⁰ Ryan V. Mishmash, Bela Bauer, Felix von Oppen, and Jason Alicea, "Dephasing and leakage dynamics of noisy Majorana-based qubits: Topological versus Andreev," *Phys. Rev. B* **101**, 075404 (2020).

⁴¹ A. Yu Kitaev, "Unpaired Majorana fermions in quantum wires," *Physics-Uspekhi* **44**, 131–136 (2001).

⁴² Suraj S. Hegde and Smitha Vishveshwara, "Majorana wave-function oscillations, fermion parity switches, and disorder in kitaev chains," *Phys. Rev. B* **94**, 115166 (2016).

⁴³ Martin Leijnse and Karsten Flensberg, "Introduction to topological superconductivity and Majorana fermions," *Semiconductor Science and Technology* **27**, 124003 (2012).

⁴⁴ Lukasz Cywiński, Roman M. Lutchyn, Cody P. Nave, and S. Das Sarma, "How to enhance dephasing time in superconducting qubits," *Phys. Rev. B* **77**, 174509 (2008).

⁴⁵ Jonas Bylander, Simon Gustavsson, Fei Yan, Fumiki Yoshihara, Khalil Harrabi, George Fitch, David G. Cory, Yasunobu Nakamura, Jaw-Shen Tsai, and William D. Oliver, "Noise spectroscopy through dynamical decoupling with a superconducting flux qubit," *Nature Physics* **7**, 565–570 (2011).

⁴⁶ O. E. Dial, M. D. Shulman, S. P. Harvey, H. Bluhm, V. Umansky, and A. Yacoby, "Charge noise spectroscopy using coherent exchange oscillations in a singlet-triplet qubit," *Phys. Rev. Lett.* **110**, 146804 (2013).

⁴⁷ Jun Yoneda, Kenta Takeda, Tomohiro Otsuka, Takashi Nakajima, Matthieu R. Delbecq, Giles Allison, Takumu Honda, Tetsuo Kodera, Shunri Oda, Yusuke Hoshi, Noritaka Usami, Kohei M. Itoh, and Seigo Tarucha, "A quantum-dot spin qubit with coherence limited by charge noise and fidelity higher than 99.9%," *Nature Nanotechnology* **13**, 102–106 (2018).

⁴⁸ Péter Boross, Gábor Széchenyi, and András Pályi, "Valley-enhanced fast relaxation of gate-controlled donor qubits in silicon," *Nanotechnology* **27**, 314002 (2016).

⁴⁹ Guilherme Tosi, Fahd A. Mohiyaddin, Vivien Schmitt, Stefanie Tenberg, Rajib Rahman, Gerhard Klimeck, and Andrea Morello, "Silicon quantum processor with robust long-distance qubit couplings," *Nature Communications* **8**, 450 (2017).

⁵⁰ Péter Boross, Gábor Széchenyi, and András Pályi, "Hyperfine-assisted fast electric control of dopant nuclear spins in semiconductors," *Phys. Rev. B* **97**, 245417 (2018).

⁵¹ Jelmer M. Boter, Xiao Xue, Tobias Krähenmann, Thomas F. Watson, Vickram N. Premakumar, Daniel R. Ward, Donald E. Savage, Max G. Lagally, Mark Friesen, Susan N. Coppersmith, Mark A. Eriksson, Robert Joyst, and Lieven M. K. Vandersypen, "Spatial noise correlations in a Si/SiGe two-qubit device from Bell state coherences," *Phys. Rev. B* **101**, 235133 (2020).

⁵² Gábor Széchenyi and András Pályi, "Parity-to-charge conversion for readout of topological Majorana qubits," *Phys. Rev. B* **101**, 235441 (2020).

⁵³ Vahid Derakhshan Maman, M.F. Gonzalez-Zalba, and András Pályi, "Charge noise and overdrive errors in dispersive readout of charge, spin, and majorana qubits," *Phys. Rev. Applied* **14**, 064024 (2020).

⁵⁴ Alexander Shnirman, Yuriy Makhlin, and Gerd Schön, "Noise and decoherence in quantum two-level systems," *Physica Scripta* **T102**, 147 (2002).

⁵⁵ Blake M. Freeman, Joshua S. Schoenfield, and HongWen Jiang, "Comparison of low frequency charge noise in identically patterned Si/SiO₂ and Si/SiGe quantum dots," *Applied Physics Letters* **108**, 253108 (2016).

⁵⁶ Bence Hetényi, Péter Boross, and András Pályi, "Hyperfine-assisted decoherence of a phosphorus nuclear-spin qubit in silicon," *Phys. Rev. B* **100**, 115435 (2019).

⁵⁷ Jan A. Krzywda and Lukasz Cywiński, "Adiabatic electron charge transfer between two quantum dots in presence of 1/f noise," *Phys. Rev. B* **101**, 035303 (2020).

⁵⁸ R. Hanson, L. P. Kouwenhoven, J. R. Petta, S. Tarucha, and L. M. K. Vandersypen, "Spins in few-electron quantum dots," *Rev. Mod. Phys.* **79**, 1217–1265 (2007).

⁵⁹ M. S. Scheurer and A. Shnirman, "Nonadiabatic processes in majorana qubit systems," *Phys. Rev. B* **88**, 064515

(2013).

⁶⁰ To obtain the smallest positive eigenvalue, we apply the `Eigenvalues` function of Wolfram Mathematica as `Eigenvalues[HBdG, 1, Method -> {"Arnoldi", "Shift" -> 0}]` in the version 12.0.0.0.

⁶¹ S. Das Sarma, Jay D. Sau, and Tudor D. Stanescu, "Splitting of the zero-bias conductance peak as smoking gun evidence for the existence of the Majorana mode in a superconductor-semiconductor nanowire," *Phys. Rev. B* **86**, 220506 (2012).

⁶² Falko Pientka, Alessandro Romito, Mathias Duckheim, Yuval Oreg, and Felix von Oppen, "Signatures of topological phase transitions in mesoscopic superconducting rings," *New Journal of Physics* **15**, 025001 (2013).

⁶³ Manisha Thakurathi, Oindrila Deb, and Diptiman Sen, "Majorana modes and transport across junctions of superconductors and normal metals," *Journal of Physics: Condensed Matter* **27**, 275702 (2015).

⁶⁴ Gilad Ben-Shach, Arbel Haim, Ian Appelbaum, Yuval Oreg, Amir Yacoby, and Bertrand I. Halperin, "Detecting Majorana modes in one-dimensional wires by charge sensing," *Phys. Rev. B* **91**, 045403 (2015).

⁶⁵ I. A. Merkulov, Al. L. Efros, and M. Rosen, "Electron spin relaxation by nuclei in semiconductor quantum dots," *Phys. Rev. B* **65**, 205309 (2002).

⁶⁶ Feliciano Giustino, Jin Hong Lee, Felix Trier, Manuel Bibes, Stephen M Winter, Roser Valentí, Young-Woo Son, Louis Taillefer, Christoph Heil, Adriana I Figueroa, Bernard Plaçais, QuanSheng Wu, Oleg V Yazyev, Erik P A M Bakkers, Jesper Nygård, Pol Forn-Díaz, Silvano De Franceschi, J W McIver, L E F Foa Torres, Tony Low, Anshuman Kumar, Regina Galceran, Sergio O Valenzuela, Marius V Costache, Aurélien Manchon, Eun-Ah Kim, Gabriel R Schleider, Adalberto Fazzio, and Stephan Roche, "The 2021 quantum materials roadmap," *Journal of Physics: Materials* **3**, 042006 (2021).

⁶⁷ Yury Makhlin, Gerd Schön, and Alexander Shnirman, "Dissipation in Josephson qubits," in *New Directions in Mesoscopic Physics (Towards Nanoscience)*, edited by R. Fazio, V. F. Gantmakher, and Y. Imry (Springer Netherlands, Dordrecht, 2003) pp. 197–224.

⁶⁸ Chia-Hsien Huang, Chih-Hwan Yang, Chien-Chang Chen, Andrew S. Dzurak, and Hsi-Sheng Goan, "High-fidelity and robust two-qubit gates for quantum-dot spin qubits in silicon," *Phys. Rev. A* **99**, 042310 (2019).

⁶⁹ Aleksei Khindanov, Dmitry Pikulin, and Torsten Karzig, "Visibility of noisy quantum dot-based measurements of Majorana qubits," *SciPost Phys.* **10**, 127 (2021).

⁷⁰ Jacob R. Colbert and Patrick A. Lee, "Proposal to measure the quasiparticle poisoning time of Majorana bound states," *Phys. Rev. B* **89**, 140505 (2014).

⁷¹ S. M. Albrecht, E. B. Hansen, A. P. Higginbotham, F. Kuemmeth, T. S. Jespersen, J. Nygård, P. Krogstrup, J. Danon, K. Flensberg, and C. M. Marcus, "Transport signatures of quasiparticle poisoning in a Majorana island," *Phys. Rev. Lett.* **118**, 137701 (2017).

⁷² Torsten Karzig, William S. Cole, and Dmitry I. Pikulin, "Quasiparticle poisoning of Majorana qubits," *Phys. Rev. Lett.* **126**, 057702 (2021).

⁷³ D I Pikulin, J P Dahlhaus, M Wimmer, H Schomerus, and C W J Beenakker, "A zero-voltage conductance peak from weak antilocalization in a Majorana nanowire," *New Journal of Physics* **14**, 125011 (2012).

⁷⁴ Haining Pan and S. Das Sarma, "Physical mechanisms for zero-bias conductance peaks in Majorana nanowires," *Phys. Rev. Research* **2**, 013377 (2020).

⁷⁵ Benjamin D. Woods, Sankar Das Sarma, and Tudor D. Stanescu, "Charge impurity effects in hybrid Majorana nanowires," (2021), arXiv:2103.06880 [cond-mat.mes-hall].

⁷⁶ Haining Pan and S. Das Sarma, "Disorder effects on majorana zero modes: Kitaev chain versus semiconductor nanowire," *Phys. Rev. B* **103**, 224505 (2021).

⁷⁷ A Vuik, D Eeltink, A R Akhmerov, and M Wimmer, "Effects of the electrostatic environment on the Majorana nanowire devices," *New Journal of Physics* **18**, 033013 (2016).

⁷⁸ Andrey E. Antipov, Arno Bargerbos, Georg W. Winkler, Bela Bauer, Enrico Rossi, and Roman M. Lutchyn, "Effects of gate-induced electric fields on semiconductor Majorana nanowires," *Phys. Rev. X* **8**, 031041 (2018).